BULLETIN OF THE POLISH ACADEMY OF SCIENCES
TECHNICAL SCIENCES, Vol. 69(2), 2021, Article number: e136735
DOI: 10.24425/bpasts.2021.136735

Effect of TiO_2 on the microstructure and phase composition of Al_2O_3 and Al_2O_3–TiO_2 APS sprayed coatings

Monika MICHALAK[1*], Leszek ŁATKA[1], Paweł SOKOŁOWSKI[1], Rolando T. CANDIDATO Jr.[2], and Andrzej AMBROZIAK[1]

[1] Faculty of Mechanical Engineering, Wroclaw University of Science and Technology, Wybrzeze Wyspianskiego 27, 50-370 Wroclaw, Poland
[2] Physics Department, College of Science and Mathematics, Mindanao State University-Iligan Institute of Technology, A. Bonifacio Avenue, Tibanga, 9200, Iligan, City, Philippines

Abstract. Plasma sprayed ceramic coatings serve as protective layers and are frequently exposed to aggressive wear, corrosion, or high-temperature environment. Currently, alumina and alumina-titania are some of the most popular protective ceramic composite coatings used in the industry. The present work deals with the investigation of the influence of TiO_2 content in the feedstock powder on the resulting microstructure and properties of Al_2O_3, $Al_2O_3 + 3$ wt% TiO_2, $Al_2O_3 + 13$ wt% TiO_2 and $Al_2O_3 + 40$ wt% TiO_2 coatings developed via atmospheric plasma spraying (APS). Specifically, the phase composition, morphology, and microstructure, as well as the mechanical and tribological performance of the coatings were examined. Results revealed that higher content of TiO_2 induced the transformation of phases, leading to the formation of intermediary Al_2TiO_5 and $Al_{2-x}Ti_{1-x}O_5$ phases. Also, the dominant α–Al_2O_3 to γ–Al_2O_3 transformation confirmed the formulation of well-melted lamellas within the coating structure. It was also shown that the increase in TiO_2 content decreased the micro-hardness of the coatings due to the formation of the intermediary phases as mentioned above and thus, affected their tribological performance. The lowest volumetric wear, equal to 7.2×10^{-5} $mm^3/(N \cdot m)$, was reported for $Al_2O_3 + 13$ wt% TiO_2 coating.

Key words: coating; atmospheric plasma spraying; Al_2O_3; TiO_2.

1. Introduction

Atmospheric plasma spraying (APS) is one of the thermal spraying techniques which allows us to produce protective coatings, typically of the thickness of 100–500 μm [1]. The method requires the feedstock in the form of micrometer-sized solid powder [2], which is transported by the carrier gas, and then injected into a hot plasma jet [3]. Subsequently, the melted powders impinge the substrate surface, forms splats, and then build the lamellar coating structure [4]. Coatings may be deposited on metallic, ceramic, or even polymeric substrates [5]. Due to the variety of available substrates and coating materials, the APS method provides a wide range of possible applications, including wear components, biomedical parts, mechanical tools, and many others [6–8].

Importantly, many of the coatings are frequently exposed to high mechanical and thermal loads [9]. But regardless of the harsh conditions they are exposed to, the coatings must preserve satisfactory mechanical, tribological and other properties [6, 10]. Such performance depends on the spraying conditions, which determine the final microstructural properties of the coatings. In our previous study [11], it was shown that the final microstructure of the coating is influenced by the powder characteristic [12]. Dense, homogeneous coatings, which provide good mechanical properties, should be sprayed with the use of powders characterized by monomodal and narrow particle size distribution.

Al_2O_3 and Al_2O_3+TiO_2 [13] are known for their good mechanical properties and favorable tribological behavior (Fig. 1) [7, 14–17]. Specifically, pure Al_2O_3 coatings are commonly

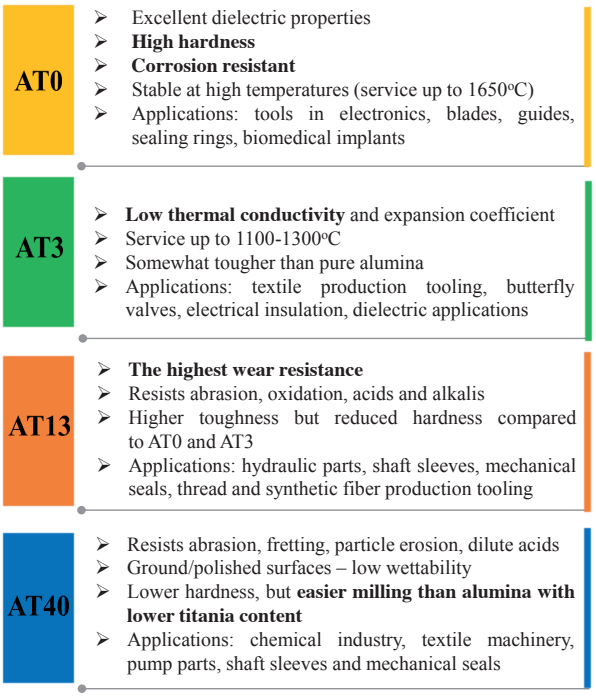

Fig. 1. Selected properties of Al_2O_3 and Al_2O_3+TiO_2 coatings [7, 14–17]

*e-mail: monika.michalak@pwr.edu.pl

Manuscript submitted 2020-09-16, revised 2020-12-11, initially accepted for publication 2021-01-20, published in April 2021

used due to their high hardness and corrosion resistance [6]. To provide increased toughness and wear resistance, TiO_2 is added to pure Al_2O_3 [18,19]. For about 50 years, the chemical composition of Al_2O_3+TiO_2 composite powders commercially available in the market is limited to 3 wt.% [20, 21], 13 wt.% [22, 23], and 40 wt.% [13, 24] of TiO_2. Some other compounds were also investigated but limited only to the individual work. Some authors mixed two separate kinds of particles and studied $Al_2O_3 + 8$ wt.% TiO_2 [25] and $Al_2O_3 + 50$ wt.% TiO_2 [26].

According to the Al_2O_3–TiO_2 phase diagram proposed by Freudenberg in 1988 [27], changes in the chemical composition of powder feedstock significantly influence the formation of coatings. Firstly, with the increased content of TiO_2, the melting temperature is lowered, which privileges the melting of the powders and provides the homogeneity of the structure [28]. Secondly, the amount of TiO_2 closed to 44%, induces the formation of the Al_2TiO_5 phase, in addition to well-known α-Al_2O_3 to γ-Al_2O_3 phase change [1, 29].

So far, a multitude of studies devoted to APS coatings of the Al_2O_3–TiO_2 system has already been carried out [11,30]. However, many papers regarding the microstructure, the mechanical and tribological performance of the coatings are limited solely to one specific chemical composition. Therefore, in this work, attention is given to the influence of TiO_2 on the phase composition, morphology, microstructure, mechanical and tribological performance of the coatings. The comparison of pure Al_2O_3 and Al_2O_3+TiO_2 coatings was also highlighted in this work.

2. Materials and methods

2.1. Powders. Four different feedstock powders were used in this study: (i) Al_2O_3, (ii) $Al_2O_3 + 3$ wt.% TiO_2, (iii) $Al_2O_3 + 13$ wt.% TiO_2 and (iv) $Al_2O_3 + 40$ wt.% TiO_2. They are labelled in the paper as: AT0, AT3, AT13 and AT40, respectively.

The following commercial micrometer-sized powders were sprayed utilizing atmospheric plasma spraying:

- Al_2O_3 Metco 6103 (Oerlikon Metco, Pfäffikon, Switzerland), agglomerated and sintered, $-45 + 15$ µm.
- $Al_2O_3 + 3$ wt.% TiO_2 AMI 6300.1 (Amil Werkstofftechnologie GmbH, Berlin, Germany), fused and crushed, $-45 + 22$ µm.
- $Al_2O_3 + 13$ wt.% TiO_2 Metco 6221 (Oerlikon Metco, Pfäffikon, Switzerland), agglomerated and sintered, $-45 + 15$ µm.
- $Al_2O_3 + 40$ wt.% TiO_2 Metco 131VF (Oerlikon Metco, Pfäffikon, Switzerland), agglomerated, $-45 + 5$ µm.

The SEM observations confirmed the results of laser diffraction (LD), see Figs. 2 and 3. Microscopic investigations were

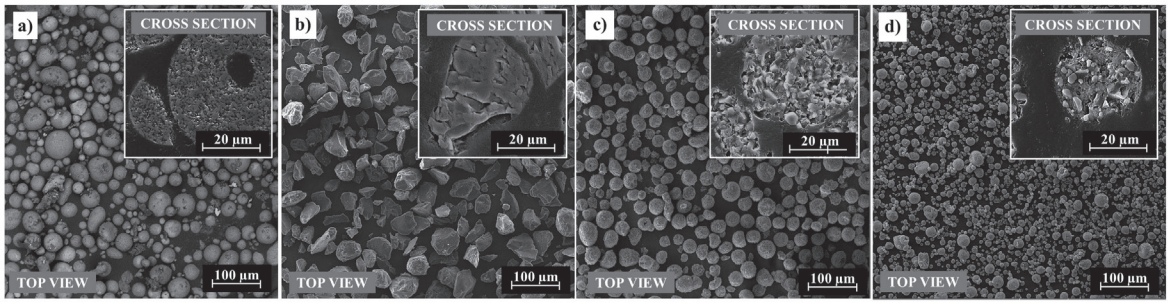

Fig. 2. Top view and cross-section images of powders used for spraying: AT0 (a), AT3 (b), AT13 (c), and AT40 (d)

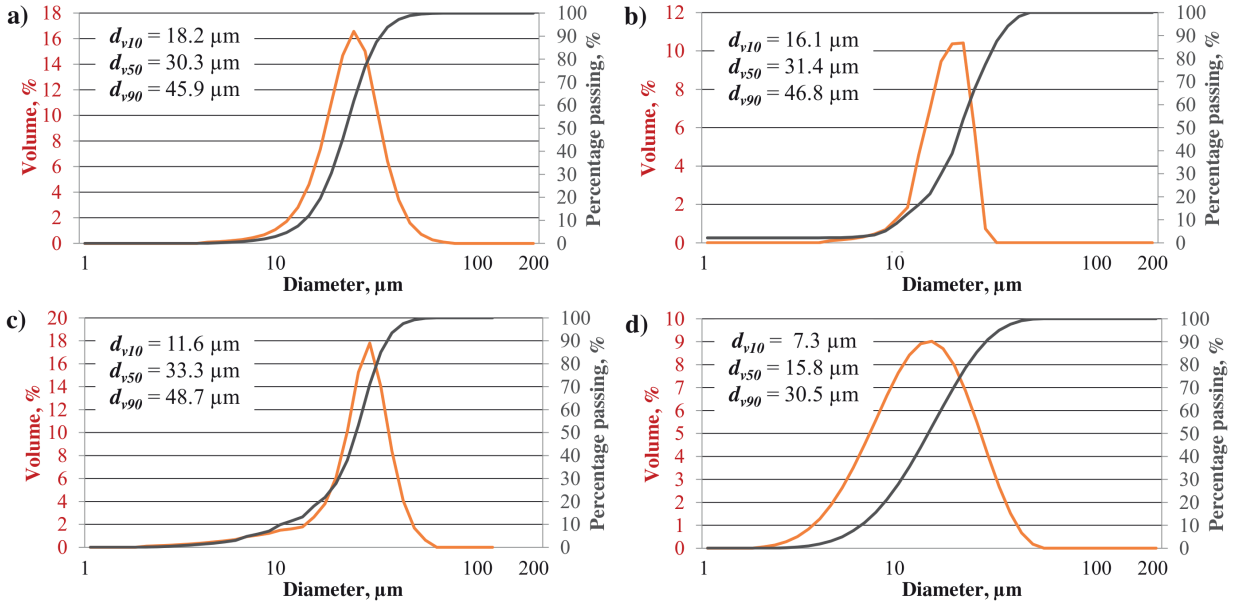

Fig. 3. Particle size distributions of powders used for spraying: AT0 (a), AT3 (b), AT13 (c), and AT40 (d)

carried out by a scanning electron microscope Phenom G2 Pro (Phenom World BV, The Netherlands). The powder particle size was evaluated by Partica LA-950V2 (Horiba, Kyoto, Japan), in accordance with the standard [31].

2.2. Spraying. The austenitic stainless steel 1.4301 (2 mm in thickness, with a diameter of 25 mm) was used as a substrate. Prior to the plasma spraying, the coupons were sand-blasted (final $R_a = 3$ µm) and cleaned in an ethanol bath. The Ni-Cr 80/20 (Amperit 250, Höganäs GmbH, Laufenburg, Germany) APS sprayed bond coats with the surface roughness of $R_a \approx 5$ µm and the thickness of around 70 µm were deposited prior to the deposition of the alumina and alumina-titania topcoats.

A conventional APS was carried out using an SG-100 torch (Praxair, Indianapolis, USA). The deposition of the coatings was accompanied by the optimization of the spraying set-up [11]. Powders were injected with a radial, external mode. The spraying parameters are given in Table 1.

Table 1
Spraying parameters of ceramic topcoats

Electrical power (kW)	35
Gas flow rate Ar/H_2 (l·min^{-1})	45/5
Stand-off distance (mm)	100
Torch scan speed (m·s^{-1})	0.3
Powder feed rate (g·min^{-1})	20

2.3. Characterization of coatings. The coatings were investigated by a scanning electron microscope Phenom G2 Pro (Phenom World BV, The Netherlands). The porosity of the samples was assessed in ImageJ free software, in accordance with ASTM E2109-01 standard [32]. The analysis was carried out for at least 20 SEM images made at 1000x magnification for each coating. The average thickness of deposits was measured on the micrographs at 500x magnification, in random areas at the coating cross-section.

The fracture morphology of the coatings was observed by a JEOL JSM-5800LV-Oxford scanning electron microscope (JEOL, Tokyo, Japan). The coatings were pre-cut and manually broken to get the fracture surface.

The X-ray diffraction data of the feedstock powders and coatings were obtained using a D8 Advance diffractometer under the Bragg–Brentano configuration with Cu K$\alpha = 0.15406$ nm radiation. A continuous scan mode with an increment of 0.02° in the scanning range of 10°−80° (2θ) was used. The content of the phases was assessed by the reference intensity ratio (RIR) technique, given in detail in [33, 34].

The roughness of the coatings was measured according to the standard [35] by profilometer MarSurf PS10 (Mahr, Göttingen, Germany). For each coating, 5 measurements of R_a, R_z, R_t parameters were carried out and then the average and the standard deviation were determined.

The microhardness of the coatings was estimated with a Vickers indenter under the load of 1.96 N (HV0.2) on a Sinowon HV-1000 apparatus (Sinowon Innovation Metrology, China), according to the standard [36]. Ten (10) indentations in random areas of the coating were made for each time. After the measurements, the average values and standard deviations were specified.

Dry sliding wear tests were carried out in a rotating unidirectional configuration, with the use of a T-01 device (ITeE-PIB, Radom, Poland), according to the standard [37]. The coatings were ground and polished before the tests to keep the Ra of free-surface below 0.8 µm. As a counterpart, polished 100Cr6 bearing steel balls with a diameter of 6 mm were used. The tests were carried out under ambient conditions, over a distance of 500 m. The other parameters used for testing were the following: a relative sliding speed of 0.1 m/s, a wear track radius of 6 mm and a normal load of 5 N. Wear traces were observed by SEM Phenom G2 Pro (Phenom World BV, The Netherlands).

3. Results and discussion

3.1. Microstructure and phase composition. The observations of coatings topography (Fig. 4) revealed a classical morphology of conventional plasma sprayed coatings [38]. On the surface, well-melted micron-sized splats, as well as semi- and even non-melted powder particles were distinguished. The last one was especially observed in the AT40 coating but some single original feedstocks were observed in AT0, probably due to the highest melting temperature among all tested powders.

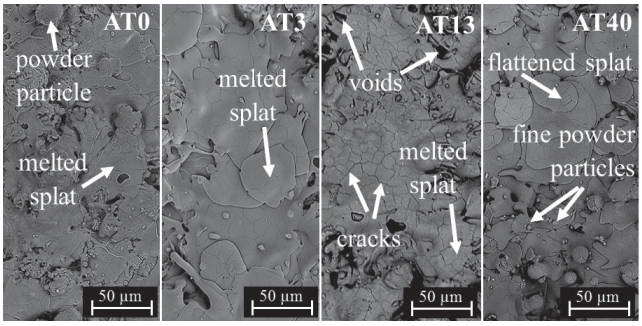

Fig. 4. SEM images of coating surface morphology

Furthermore, it is supposed that AT40 powder fragmented and disaggregated during spraying – many fine, non-aggregated particles were observed in the top surface of AT40 coating. This was not found for AT0, AT3 and AT13 particles, characterized by different production conditions: AT0 and AT13 – agglomerated and sintered; AT3 – fused and crushed (this powder is not available on the market in the agglomerated state); AT40 – only agglomerated. The agglomerating and sintering process provided stronger binding and thus, easier transport of the material during AT0 and AT13 APS spraying. A similar trend of good bond strength (and consequently – unproblematic feeding) was observed also for AT3 powder. Currently, commercially available spheroidal AT40 powders are manufactured only in the agglomerated form, without sintering. Thus, AT40 particles debonded the most easily and were easily directed to-

wards the periphery of plasma jet, characterized by lower temperature. Hence, some re-solidified or even non-melted powder particles were observed.

The cross-section micrographs (Fig. 5) showed that all coatings well adhered to the bond coat layer. The interface between alumina or alumina-titania topcoats and NiCr bond coats is free of any cracks, pores, or discontinuities. Coatings revealed a similar thickness, in the range between 186 μm and 201 μm, which provided similar deposition efficiencies as the coatings were sprayed with a similar number of spray cycles each time (Table 2). The microstructure of coatings was relatively homogeneous, free of inter- or intra-lamellar cracks, and with some content of porosity, which is typical for plasma-sprayed coatings. It was observed that the pores were of various sizes (ranging from a micrometer to a nanometer) and were homogeneously distributed along the coating cross-section.

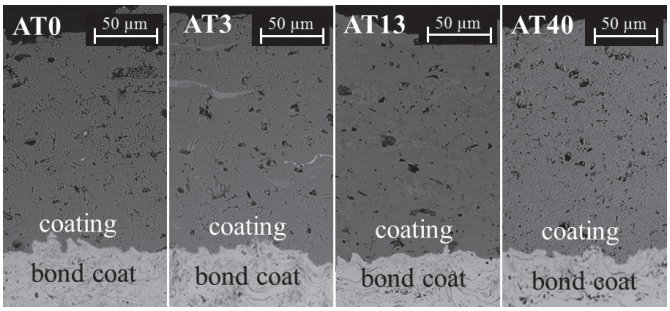

Fig. 5. SEM images showing cross-sections of deposited coatings

Table 2
Average thickness and porosity of deposited Al_2O_3 and Al_2O_3–TiO_2 coatings

	AT0	AT3	AT13	AT40
Thickness (μm)	189 ± 9	201 ± 7	198 ± 6	186 ± 5
Thickness per pass (μm/pass)	24	25	25	23
Porosity (vol. %)	14 ± 1	9 ± 1	13 ± 1	12 ± 1

The values of porosity are given in Table 2. No direct relationship was observed between the TiO_2 content and porosity. However, the influence of the manufacturing route of the powders cannot be neglected. It was reported that powder feedstock of the same chemical composition, but made by different techniques, may influence the properties of the final coating [13]. It was shown that the melting of the powder depends not only on the melting point (resulting from the chemical composition) but is also influenced by a thermal conductivity of the particle itself. Wang et al. [39] has shown that the fused and crushed feedstock powder, which consisted of mechanical blends of separately fused Al_2O_3 and TiO_2 particles, was characterized by better thermal conductivity than the Al_2O_3+TiO_2 powder in the agglomerated form. The poor thermal conductivity led to the increased porosity of the coating [40]. As a result, an AT3 coating exhibited a higher melting and lower porosity than AT13 and AT40 coatings. Nevertheless, when the porosity of the coatings is compared based on the agglomerated powders, it could be seen that with the increased content of TiO_2, the porosity of the coatings is slightly decreased.

Fig. 6 shows SEM micrographs of fracture surfaces. Although all of the investigated samples were built of finely structured powders, the observed surfaces showed some differences. For AT0, the lamellar structure was clearly visible, and the columnar grains were obviously observed, which was caused by rapid cooling rates upon the particle deposition. AT3 revealed the smoothest fracture surface when compared with AT0, AT13, and AT40, with well-flattened splats. This may be attributed to a different powder morphology of AT13. The fractures of AT13 and AT40 also exhibited a typical structure for plasma spraying. However, some single fine pores for AT13 were observed. Finally, the fracture surface of AT40 consisted of regions with a different melting degree. Unlike in the AT0 and AT3 lamellar fractures, a bimodal morphology, containing melted and non-melted fine powder residues were retained in the coating. Additionally, single micro-sized voids were observed, which were induced by the presence of loosely bonded powders.

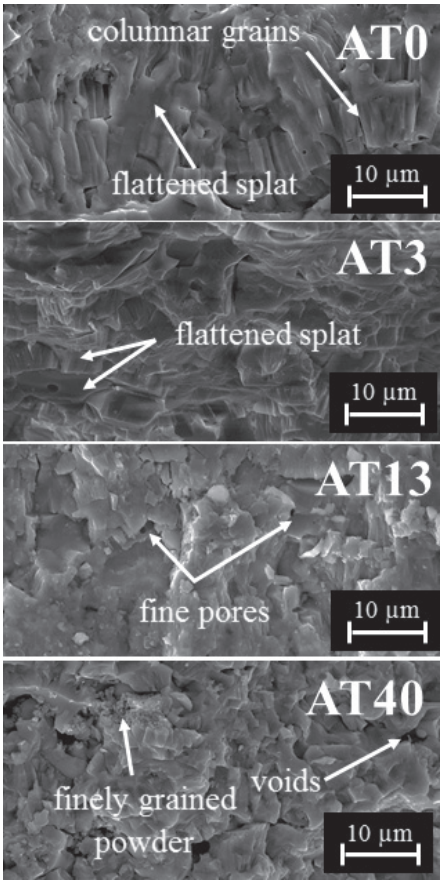

Fig. 6. SEM micrograph of the fractured surfaces in deposited coatings

Fig. 7 presents the phases identified in powders (Fig. 7a) and APS sprayed coatings (Fig. 7b). AT0 particles contained 100% of thermodynamically stable α-Al_2O_3. In the case of

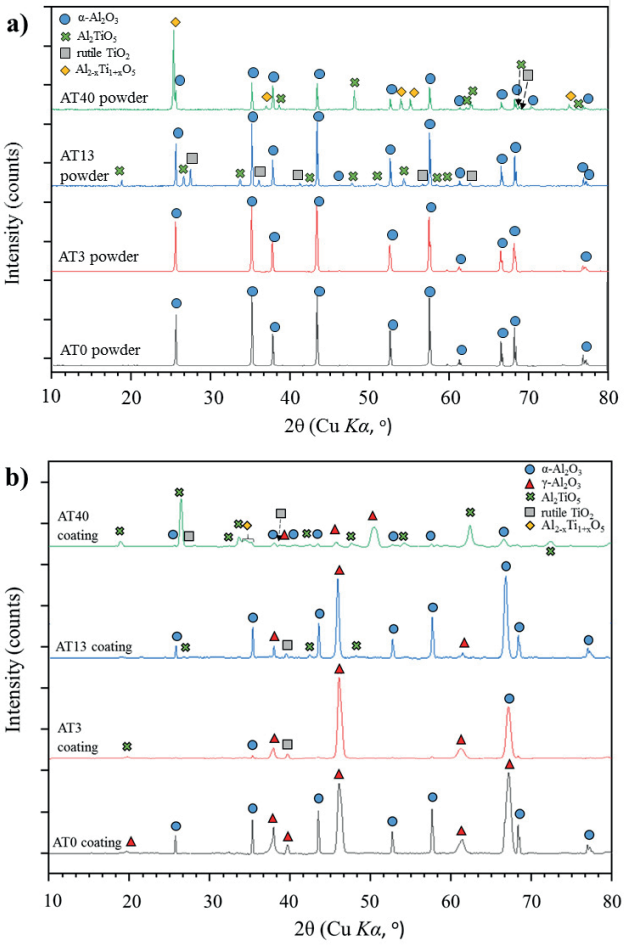

Fig. 7. XRD patterns of powders used for APS spraying (a) and deposited coatings (b)

AT3 powder, a diffraction analysis also revealed only peaks of α-Al_2O_3, and the results were confirmed by a quantitative evaluation, given in Fig. 8. It is assumed that in this powder, some TiO_2-related phases might be present, but their concentration was not enough to be detected by XRD. AT13 and AT40 powders, in addition to α-Al_2O_3 phase, also contained: rutile-TiO_2 (AT13, AT40), tialite Al_2TiO_5 (AT13, AT40), and $Al_{2-x}Ti_{1+x}O_5$ (AT40). Similar phase compositions were found in other studies [3, 6, 41].

After spraying the powders, phase changes occurred. In the case of AT0 coatings, the transformation of α-Al_2O_3 into γ-Al_2O_3 was reported, due to lower nucleation energy of γ-Al_2O_3 and the rapid cooling of the splats [42, 43]. The α-Al_2O_3 remained in the coating due to the presence of semi-melted powder particles, as confirmed by the previous SEM observations (Fig. 4). In AT3 coatings, the content of α-Al_2O_3 (25 vol.%) was significantly reduced with an appearance of γ-Al_2O_3 (72 vol.%), accompanied by a formation of a small amount of Al_2TiO_5 (3 vol.%). The results confirmed then the high degree of powders melting [44], as already discussed in the context of porosity evaluation. In AT13 coatings, the changes were even more complex. Beyond the common transformation of α-Al_2O_3 into γ-Al_2O_3 (before spraying – 83 vol.%, after – 53 vol.% of α-Al_2O_3), it was observed that tialite (Al_2TiO_5) was reduced significantly (from initial 10 vol.% to 5 vol.%). Additionally, rutile-TiO_2 was not observed in the coating (which was found in the as-produced powder). This resulted probably from the use of Ar/H_2 gases for the spraying process, which led to the reduction of TiO_2 phases [13]. Also, the AT40 coating revealed different phase composition when compared with the feedstock powder. The dominating phase was tialite Al_2TiO_5 (40 vol.%), and that was clearly related to the Al_2O_3–TiO_2 diagram [45]. Tialite originated from a reaction between Al_2O_3 and TiO_2 in the hot plasma plum. Additionally, its formation was promoted by the fine size of AT40 particles, characterized by a larger surface area [27, 46, 47]. In the agglomerated powder, the total contact surface area between Al_2O_3 and TiO_2 is very high due to the small size of the primary particles. In that case, Al_2O_3 and TiO_2 react together and form Al_2TiO_5. A significant reduction of the intermediate phase $Al_{2-x}Ti_{1+x}O_5$ was also found, due to the oxidization and decomposition into Al_2TiO_5, [13].

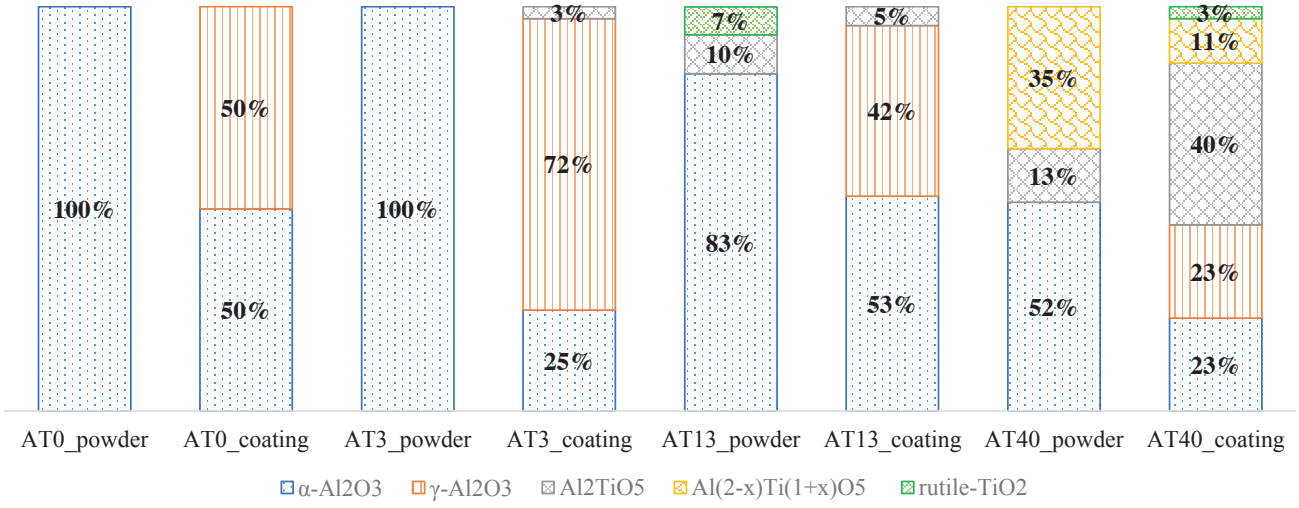

Fig. 8. Quantitative estimation of the phases composition in powders and coatings

3.2. Roughness. Fig. 9 represents the average surface roughness of the as-sprayed coatings. Amongst all coatings, AT40 revealed the lowest roughness parameters. This stemmed from the deposition of finer particles, which had already broken during feeding to the plasma jet. Smaller powders tend to generate a surface of lower roughness [48]. R_a, R_z, and R_t parameters obtained for AT0, AT3, and AT13 coatings were similar, which is caused by the factors influencing the roughness most effectively (namely: plasma power, carrier gas flow rate, and rotation velocity of the substrate during spraying [24, 49]), were kept at a constant level. The sizes of AT0, AT3 and AT13 particles were similar to each other and thus resulted in similar roughness of the deposited coatings.

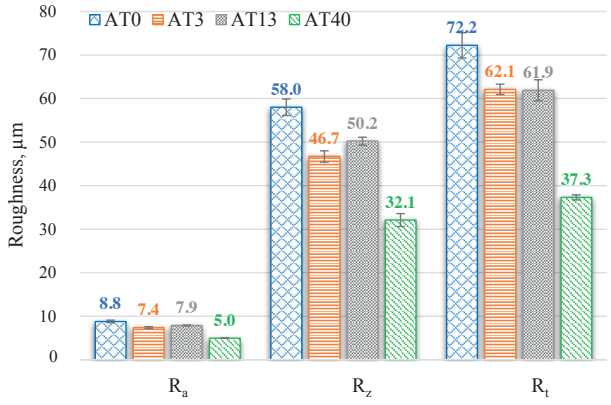

Fig. 9. Average roughness of sprayed coatings

3.3. Microhardness. The results of microhardness measurements (Fig. 10) clearly indicated that HV0.2 decreased with the increased content of TiO_2. At the same time, it was observed that the AT13 coating with the highest content of a hard and brittle α-Al_2O_3 phase in the final deposit was characterized by a low decrease of hardness when compared with an AT3 coating [50]. Thus, the effect of the porosity on the hardness was limited by the effect of the phase composition [30].

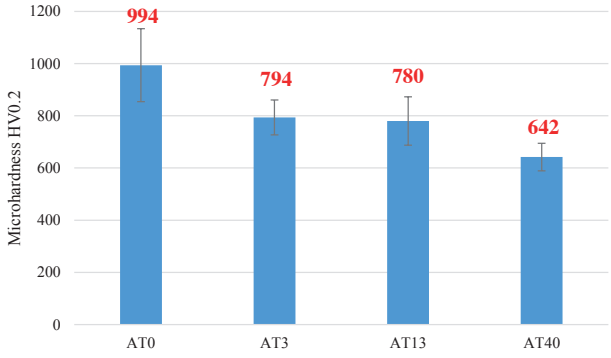

Fig. 10. Average Vickers microhardness of sprayed coatings

The estimated hardness values corresponded well with the results given in the literature. For example, Yilmaz et al. [26] reported the hardness of $Al_2O_3 + 13$ wt.% TiO_2 coatings equal to 853 HV0.2, whilst $Al_2O_3 + 40$ wt.% TiO_2 – equal to 566 HV0.2. Similar values were given also by Yugeswaran et al. [21].

3.4. Wear resistance. Ball-on-disk tests revealed that the AT13 coating was displaying the best tribological behavior amongst all the sprayed coatings, with the volumetric wear equal to 7.2×10^{-5} mm^3/(N·m) (see Fig. 11). Moreover, this coating was characterized by the lowest scatter of standard deviation.

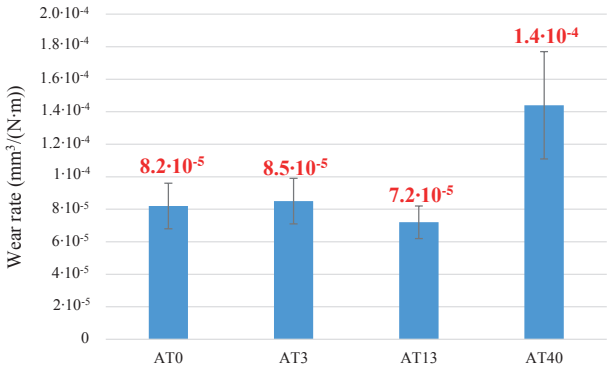

Fig. 11. Average volumetric wear of sprayed coatings

The wear mechanism of the coatings was studied by SEM analysis, which is presented in Fig. 12. In the case of AT0 and AT3 coatings (see example in Figs. 12a–12b, respectively), the main wear mechanism was low cycle fatigue, accompanied by splats delamination. This cyclic fatigue was characterized by the cracking of the coating, the delamination of the material, and its smearing through the wear trace. In the case of the AT3 coating, a lot of debris and cracks are visible, as well as some scratches. The wear of the AT13 coating was different (see Fig. 12c) – a more adhesive mode was observed. However, numerous cracks were observed in the wear trace, and therefore, similar low cycle fatigue was observed. It was intensified by the spallation and smearing of the debris material. The highest wear resistance of the AT13 coating was related to its low friction coefficient (Table 3) and hard structure (high content of α-Al_2O_3 phase). For AT40, the friction coefficient was higher, while the hardness and content of α-Al_2O_3 phase were lower than for AT13. Additionally, it was observed that detachment of coatings was mainly initiated at the splat boundaries and areas of uniformities. In Fig. 12d there are some micro-scratching and spallation areas. In places where non-fully melted and resolidified particles were removed, the relatively soft material (high content of an Al_2TiO_5 phase) was smeared on the surface and fill these areas. Therefore, the AT40 coating was worn the most intensively. A similar trend was observed also by Szala

Table 3
Average values of friction coefficients of deposited coatings

	AT0	AT3	AT13	AT40
Friction coefficient μ	0.68 ± 0.04	0.59 ± 0.03	0.57 ± 0.03	0.66 ± 0.03

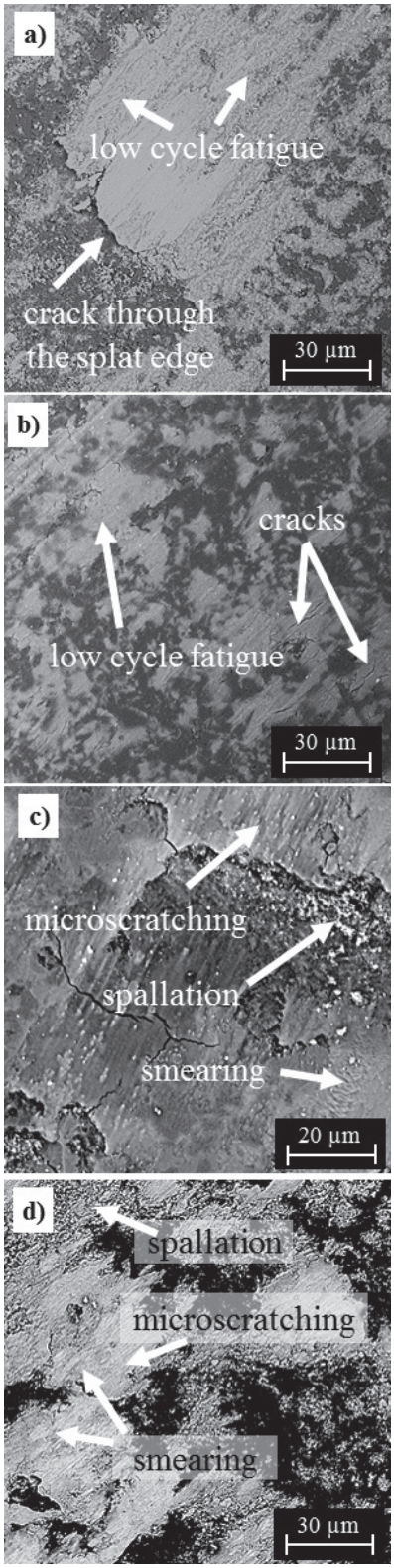

Fig. 12. Wear tracks of AT0 (a), AT3 (b), AT13 (c) and AT40 (d) coatings

et al. [51], who investigated TiO_2-based APS coatings. The authors concluded that the brittle cracking of the lamellas had an impact on the wear behavior of the layer.

The wear resistance of the coatings was related to the phases which remained after spraying the powder feedstocks. The dominant phases in AT0, AT3, and AT13 coatings were α-Al_2O_3 and γ-Al_2O_3. The AT3 coating contained only 25 vol.% of α-Al_2O_3, whilst in AT0 one alpha phase content was equal to 50 vol.%, which apparently influenced the microhardness values. On the other hand, the porosity of AT3 was significantly lower than that of AT0, and it could be a reason why similar volumetric wear of the AT0 and AT3 coatings was obtained. In this case, the powders were melted only partially; that is, the outer surface of the powders melted and solidified rapidly (in the form of γ-Al_2O_3 phase, of relatively lower hardness and higher toughness than α-Al_2O_3), whilst the core of the powder was unchanged (in the form of hard α-Al_2O_3). Therefore, the coatings revealed the structure that was built of the γ-Al_2O_3 matrix, strengthened by α-Al_2O_3 [52]. Additionally, low wear of the AT13 coating influenced by the decrease in the coating hardness with TiO_2 is added in Al_2O_3 powder, as confirmed also by other authors [49]. The AT40 coating was worn the most intensively (1.4×10^{-4} mm^3/(N·m), which is consistent with having the lowest microhardness amongst all coatings.

4. Conclusions

In this paper, the APS spraying with feedstock powders having chemical compositions: Al_2O_3, Al_2O_3+3 wt.% TiO_2, Al_2O_3 + 13 wt.% TiO_2, and Al_2O_3 + 40 wt.% TiO_2 was carried out. The coatings were studied in terms of the influence of TiO_2 content on the microstructure, phase composition, as well as the chosen mechanical and tribological properties. To summarize, the following can be stated:

- All the coatings revealed a topography and microstructure typical for APS sprayed coatings, with cracks, pores, and voids. It was observed that powder melting depends not only on TiO_2 content but is influenced by its characteristics resulting from the manufacturing route.
- XRD studies showed that all the powders underwent phase transformations during spraying. With the increased content of TiO_2, the number of phases related to pure Al_2O_3 (α-Al_2O_3 and γ-Al_2O_3) was considerably decreased, whilst the number of TiO_2-phases (rutile-TiO_2, Al_2TiO_5, $Al_{(2-x)}Ti_{(1+x)}O_5$) increased.
- The clear trend of the decrease in Vickers hardness was observed in the coatings with an increased amount of TiO_2, due to the presence of more phases derived from TiO_2. The highest hardness of 994 HV0.2 was obtained for Al_2O_3, characterized also by the highest content of α-Al_2O_3 (50 vol.%) in the final coating.
- The wear resistance of the coatings was influenced both by the decreased hardness of the coatings with increased TiO_2 content, as well as different phase compositions of the as-sprayed coatings. The AT13 coating showed the best tribological performance, due to the combined effect of favorable hardness and the microstructure consisting of an γ-Al_2O_3 matrix, strengthened by α-Al_2O_3 particles.

Acknowledgements. Dr. Rafał Flamholc from Anton Paar company is thankfully acknowledged for the dynamic light scattering measurements. Prof. Mariusz Walczak from Lublin University of Technology is also acknowledged for his support in ball-on-disk testing.

References

[1] A. Richter, L.-M. Berger, S. Conze, Y.J. Sohn, and R. Vassen, "Emergence and impact of Al_2TiO_5 in Al_2O_3–TiO_2 APS coatings", *IOP Conf. Series: Mater. Sci. Eng.* 480, 012007 (2019).

[2] L. Pawłowski, *The Science and Engineering of Thermal Spray Coatings*, 2nd ed., Wiley, Chichester, 2008.

[3] S. Islak *et al.*, "Effect on microstructure of TiO_2 rate in Al_2O_3–TiO_2 composite coating produced using plasma spray method", *Optoelectron. Adv. Mat.* (9–10), 844–849 (2013).

[4] J. Zimmerman, Z. Lindemann, D. Golański, T. Chmielewski, and W. Włosiński, "Modeling residual stresses generated in Ti coatings thermally sprayed on Al_2O_3 substrates", *Bull. Pol. Acad. Sci. Tech. Sci.* 61(2), 515–525 (2013)

[5] K. Kudła and J. Iwaszko, "Surface modification of ZrO2–10 wt.% CaO plasma sprayed coating", *Bull. Pol. Acad. Sci. Tech. Sci.* 64(4), 937–942 (2016).

[6] D. Franco, H. Ageorges, E. Lopez, and F. Vargas, "Tribological performance at high temperatures of alumina coatings applied by plasma spraying process onto a refractory material", *Surf. Coat. Technol.* 371, 276–286 (2019).

[7] S. Mehar, S. Sapate, N. Vashishtha, and P. Bagde, "Effect of Y2O3 addition on tribological properties of plasma sprayed Al_2O_3–13% TiO_2 coating", *Ceram. Int.* 46, 11799-11810 (2020).

[8] J. Rolando T. Candidato Jr., P. Sokołowski, L. Łatka, S. Kozerski, L. Pawłowski, and A. Denoirjean, "Plasma spraying of hydroxyapatite coatings using powder, suspension and solution feedstocks", *Weld. Techn. Rev.* 87(10), 64–71 (2015).

[9] M. Winnicki, T. Piwowarczyk, and A. Małachowska, "General description of cold sprayed coatings formation and of their properties", *Bull. Pol. Acad. Sci. Tech. Sci.* 66(3), 301–310 (2018).

[10] K. Pietrzak, A. Strojny-Nędza, A. Gładki, S. Nosewicz, D. Jarząbek, and M. Chmielewski, "The effect of ceramic type reinforcement on structure and properties of Cu-Al_2O_3 composites", *Bull. Pol. Acad. Sci. Tech. Sci.* 66 (4), 553–560 (2018).

[11] M. Michalak, L. Łatka, P. Sokołowski, A. Niemiec, and A. Ambroziak, "The microstructure and selected mechanical properties of Al_2O_3 + 13 wt.% TiO_2 plasma sprayed coatings", *Coatings* 10 (2), 173 (2020).

[12] M. Chmielewski and K. Pietrzak, "Metal-ceramic functionally graded materials – manufacturing, characterization, application", *Bull. Pol. Acad. Sci. Tech. Sci.* 64(1), 151–160 (2016).

[13] A. Richter, L.-M. Berger, Y. Sohn, S. Conze, K. Sempf, and R. Vaßen, "Impact of Al_2O_3–40 wt.% TiO_2 feedstock powder characteristics on the sprayability, microstructure and mechanical properties of plasma sprayed coatings", *J. Eur. Ceram. Soc.* 39(16), 5391–5402 (2019).

[14] Material Product Data Sheet High Purity Aluminum Oxide Thermal Spray Powders – Oxide Ceramic Powder Materials for Thermal Spray – Oerlikon Metco.

[15] Material Product Data Sheet Alumina 3% Titania Thermal Spray Powders – Oxide Ceramic Powder Materials for Thermal Spray – Oerlikon Metco.

[16] Material Product Data Sheet Aluminum Oxide 13% Titanium Dioxide Powders – Oxide Ceramic Powder Materials for Thermal Spray – Oerlikon Metco.

[17] Material Product Data Sheet Aluminum Oxide 40% Titanium Dioxide Powders – Oxide Ceramic Powder Materials for Thermal Spray – Oerlikon Metco.

[18] H. Li, Z. Ke, J. Li, L. Xue, and Y. Yan , "An effective low-temperature strategy for sealing plasma sprayed Al_2O_3-based coatings", *J. Eur. Ceram. Soc.* 38(4), 1871–1877 (2018).

[19] A. Šuopys, L. Marcinauskas, R. Kėželis, M. Aikas, and R. Uscila, "Thermal and chemical resistance of plasma sprayed Al_2O_3, Al_2O_3–TiO_2 coatings", *Res. Sq.*, (to be published).

[20] M. Djendel, O. Allaoui, R. Boubaaya, "Characterization of alumina-titania coatings produced by atmospheric plasma spraying on 304 SS steel", *Acta Phys. Pol.* 132 (3), 538–540 (2017).

[21] S. Yugeswaran, V. Selvarajan, M. Vijay, P. Ananthapadmanabhan, and K. Sreekumar, "Influence of critical plasma spraying parameter (CPSP) on plasma sprayed alumina–titania composite coatings", *Ceram. Int.* 36 (1), 141–149 (2010).

[22] W. Żórawski, A. Góral, O. Bokuvka, L. Lityńska-Dobrzyńska, and K. Berent, "Microstructure and tribological properties of nanostructured and conventional plasma sprayed alumina–titania coatings", *Surf. Coat. Technol.* 268, 190–197 (2015).

[23] W. Tian, Y. Wang, and Y. Yang, "Three body abrasive wear characteristics of plasma sprayed conventional and nanostructured Al_2O_3–13%TiO_2 coatings", *Tribol. Int.* 43(5–6), 876–881 (2010).

[24] T. Rajesh and R. Rao "Experimental investigation and parameter optimization of Al_2O_3–40%TiO_2 atmospheric plasma spray coating on SS316 steel substrate", *Mater. Today: Proc.* 5 (2), 5012–5020 (2018).

[25] E. Song, J. Ahn, S. Lee, and N. Kim, "Effects of critical plasma spray parameter and spray distance on wear resistance of Al_2O_3–8 wt.% TiO_2 coatings plasma-sprayed with nanopowders", *Surf. Coat. Technol.* 202(15), 3625–3632 (2008).

[26] R. Yilmaz, A. Kurt, A. Demir, and Z. Tatli, "Effects of TiO_2 on the mechanical properties of the Al_2O_3–TiO_2 plasma sprayed coating", *J. Eur. Ceram. Soc.* 27(2–3), 1319–1323 (2007).

[27] F. Freudenberg, "Study of the reaction to the solid state Al_2O_3 + TiO_2 → Al_2TiO_5: structure observation", thesis at University Lausanne (1988) [in French].

[28] E. Klyatskina *et al.*, "Sliding wear behavior of Al_2O_3–TiO_2 coatings fabricated by the suspension plasma spraying technique", *Tribol. Lett.* 59(8), 1–9 (2015).

[29] H. Ageorges and P. Ctibor, "Comparison of the structure and wear resistance of Al_2O_3–13 wt.% TiO_2 coatings made by GSP and WSP plasma process with two different powders", *Surf. Coat. Technol.* 202(18), 4362–4368 (2008).

[30] N. Dejang, A. Watcharapasorn, S. Wirojupatump, P. Niranatlumpong, and S. Jiansirisomboon, "Fabrication and properties of plasma-sprayed Al_2O_3/TiO_2 composite coatings: a role of nano-sized TiO_2 addition", *Surf. Coat. Technol.* 204 (9–10), 1651–1657 (2010).

[31] ASTM B822 – 17 Particle Size Distribution of Metal Powders and Related Compounds by Light Scattering, ASTM International: West Conshohocken, PA, USA (2017).

[32] ASTM E2109-01 01 Standard Test Methods for Determining Area Percentage Porosity in Thermal Sprayed Coatings, ASTM International: West Conshohocken, PA, USA (2014).

[33] P.S. Prevéy, "X-ray diffraction characterization of crystallinity and phase composition in plasma-sprayed hydroxyapatite coatings", *J. Therm. Spray. Tech.* 9, 369–376 (2000).

[34] L. Marcinauskas and P. Valatkevičius, "The effect of plasma torch power on the microstructure and phase composition of alumina coatings", *Mat. Sci.–Poland* 28, 451–458 (2010).

[35] EN ISO 4288:1996 Geometrical Product Specifications (GPS) – Surface texture: Profile method – Rules and procedures for the assessment of surface texture (1996).

[36] EN ISO 4516: 2004 Metallic and other inorganic coatings – Vickers and Knoop microhardness tests (2004).

[37] ASTM G99-17 Standard Test Method for Wear Testing with a Pin-on-Disk Apparatus,ASTM International: West Conshohocken, PA, USA (2017).

[38] P. Bandyopadhyay, D. Chicot, B. Venkateshwarlu, V. Racherla, X. Decoopman and J. Lesage, "Mechanical properties of conventional and nanostructured plasma sprayed alumina coatings", *Mech. Mater.* 53, 61–71 (2012).

[39] M. Wang and L. Shaw, "Effects of the powder manufacturing method on microstructure and wear performance of plasma sprayed alumina–titania coatings", *Surf. Coat. Technol.* 202(1), 34-44 (2007).

[40] I. Ahmed and T. Bergman, "Three-dimensional simulation of thermal plasma spraying of partially molten ceramic agglomerates", *J. Therm. Spray. Tech.* 9, 215–224 (2000).

[41] M. Michalak, F.-L. Toma, L. Latka, P. Sokolowski, M. Barbosa, and A. Ambroziak, "A study on the microstructural characterization and phase compositions of thermally sprayed Al_2O_3–TiO_2 coatings obtained from powders and water-based suspensions", *Materials* 13(11), 2638 (2020).

[42] R. McPherson, "Formation of metastable phases in flame- and plasma-prepared alumina", *J. Mater. Sci.* 8, 851–858 (1973).

[43] F.-L. Toma, L.-M. Berger, C. Stahr, T. Naumann, and S. Langner, "Microstructures and functional properties of suspension-sprayed Al_2O_3 and TiO_2 coatings: an overview", *J. Therm. Spray. Tech.* 19, 262–274 (2010).

[44] F. Dachille, P. Simons, and R. Roy, "Pressure-temperature studies of anatase, brookite, rutile and TiO2-II", *Am. Mineral.* 53, 1929–1939 (1968).

[45] D. Goldberg, "Contribution to study of systems formed by alumina and some oxides of trivalent and tetravalent metals especially titanium oxide", *Revue Internationale Des Hautes Temperatures et Des Refractaires* 5, 181–182 (1968).

[46] L.-M. Berger, K. Sempf, Y. Sohn, and R. Vaßen, "Influence of feedstock powder modification by heat treatments on the properties of APS-sprayed Al_2O_3–40%TiO_2 coatings", *J. Therm. Spray. Tech.* 27, 654–666 (2018).

[47] S. Hoffmann, S. Norberg, and M. Yoshimura, "Melt synthesis of Al_2TiO_5 containing composites and reinvestigation of the phase diagram Al_2O_3–TiO_2 by powder X-ray diffraction", *J. Electroceram.* 16, 327–330 (2006).

[48] S. Goel, S. Björklund, N. Curry, U. Wiklund, and S. Joshi, "Axial suspension plasma spraying of Al_2O_3 coatings for superior tribological properties", *Surf. Coat. Technol.* 315, 80–87 (2017).

[49] M. Ghazali, S. Forghani, N. Hassanuddin, A. Muchtar, and A. Daud, "Comparative wear study of plasma sprayed TiO_2 and Al_2O_3–TiO_2 on mild steels", *Tribol. Int.* 93, 681–686 (2016).

[50] E. Jordan *et al.*, "Fabrication and evaluation of plasma sprayed nanostructured alumina–titania coatings with superior properties", *Mater. Sci. Eng. A* 301(1), 80–89 (2001).

[51] M. Szala, A. Dudek, A. Maruszczyk, M. Walczak, J. Chmiel, and M. Kowal, "Effect of atmospheric plasma sprayed TiO_2–10%NiAl cermet coating thickness on cavitation erosion, sliding and abrasive wear resistance", *Acta Phys. Pol. A.* 136, 335–341 (2019).

[52] S. Yao, Y. Su, H. Shu, C. Lee, and Z. You, "Comparative study on nano-structural and traditional Al_2O_3–13TiO_2 air plasma sprayed coatings and their thermal shock performance", *Key Eng. Mater.* 739, 103–107 (2017).